JOURNAL OF MATERIALS SCIENCE **34** (1999) 5955–5959

Characterization of strength and microstructure in deformation processed Al-Mg composites

K. XU, A. M. RUSSELL, L. S. CHUMBLEY, F. C. LAABS,
V. B. GANTOVNIK, Y. TIAN
206 Wilhelm Hall, Ames Laboratory and Department of Materials Science & Engineering, Iowa State University, Ames, IA 50011
E-mail: xukai@iastate.edu

The microstructures, mechanical properties and electrical resistivity have been evaluated for deformation processed Al-20 vol % Mg and Al-13 vol % Mg composites. The Mg second phase adopts a convoluted, ribbon shape filamentary morphology after deformation. Both the size and spacing of these filaments decreases with deformation. The strength of these composites increases exponentially with reduced spacing of Mg filaments. The electrical resistivity of these Al-Mg composites is slightly higher than that of pure Al.

1. Introduction

Deformation processed metal matrix composites (DMMCs) formed by mechanical working (i.e., rolling, swaging, or wire drawing) of two-phase ductile metal mixtures have received considerable study in recent years because of the unique properties they show compared to conventional materials. Previous studies showed anomalous strengthening in face centered cubic (FCC) matrix materials such as Cu [1–3] and Al [4] containing body centered cubic (BCC) second phase. The bcc second phase develops a ⟨110⟩ fiber texture, which limits the bcc phase to plane strain. Some recent studies of Ti-Y [5, 6], Mg-Ti [7], Al-Ti [8] have shown hexagonal close packed (HCP) metals' potential application in DMMC's. The HCP metals Ti and Y develop a $\langle 10\bar{1}0 \rangle$ wire texture when axisymmetrically deformed. This texture restricts the HCP phase to plain strain, which means that a fcc matrix containing HCP second phase material will deform in a similar way to that of FCC/BCC composites.

In this study, a fcc matrix Al containing HCP Mg was examined to further explore the relationship between properties and microstructures in FCC/HCP DMMC's and to see if a useful engineering material might result.

2. Experimental procedures

High purity Al powder (99.99% purity, particle size of 45–75 μm, produced by the gas atomized rapid solidification method at Ames Laboratory) was mixed with Mg powder (99.80% purity, particle size smaller than 45 μm). These two powders were mixed and cold isostatically pressed (CIP'ed) at 132 MPa. There were two compositions for the Al-Mg composites. One was 80 vol % Al-20 vol % Mg, which is referred to as Al-20Mg; the other was 87 vol % Al-13 vol % Mg, which was referred to as Al-13Mg. The 37 mm diameter green compacts were loaded into a Ta-foil-lined, OFHC Cu can which was soldered shut and evacuated. The copper cans and enclosed specimen were extruded at room temperature through a 25.4 mm diameter die followed by water quenching. The true strain of these specimens can be calculated with: $\eta = 2 \ln(d_0/d)$, where d_0 and d are the initial and final specimen diameter respectively.

The extruded Al-20Mg rod with Cu sleeve was swaged at room temperature to a diameter of 12.7 mm ($\eta = 2.77$). At this point the Cu and Ta were removed by machining. The bare Al-20Mg was swaged to a diameter of 4.1 mm ($\eta = 4.37$). One small piece of the $\eta = 4.37$ sample was swaged to 1.6 mm ($\eta = 6.29$) while most of the $\eta = 4.37$ rods were set aside for a second extrusion. Metallography coupons and two tensile specimens were cut from the specimen at $\eta = 2.77$, 4.37 and 6.29.

The 4.1 mm diameter Al-20Mg rods were cleaned with acetone, cut to 34.3 mm length, and bundled inside another Ta-foil-lined, OFHC Cu can. This Cu can was soldered and evacuated. The 51 mm outside diameter, 182 mm long Cu can was extruded at room temperature through a 25.4 mm die followed by water quenching. During the second extrusion, the separate rods bonded together into a single piece with an cumulative deformation ratio of 5.47. The extruded rod was then swaged to a diameter of 3.2 mm, at which point the Cu and Ta were removed by machining. The bare Al-20Mg rod was swaged at 300 K to diameters of 1.8 mm ($\eta = 10.13$), and 1 mm ($\eta = 11.25$). Small metallography coupons and two tensile specimens were cut from the specimen at $\eta = 10.13$ and 11.25.

The extruded Al-13Mg rod with Cu sleeve was processed similarly with some minor variation in η values for tensile test and metallography coupons.

Tensile tests were performed for all specimens with $\eta < 6$ following ASTM standard E8 [9]. For smaller diameter wires with $\eta > 6$, tensile specimens were made

by embedding the wire ends into Cu sleeves using adhesive. All tensile tests were done at room temperature with a strain rate of 1.0 mm/min (when $\eta < 6$), and 0.15 mm/min (when $\eta > 6$).

Filament thickness and spacing were determined by standard stereographic intercept procedures [10] using a JOEL6100 SEM.

Four point electrical resistance measurement was performed for Al-13Mg specimen ($\eta = 11.28$) before and after annealing at 538 K in vacuum for 1 h and for Al-20Mg ($\eta = 11.95$) without annealing.

3. Results and discussion

3.1. Microstructure characterization

Figs 1, 2 show the SEM micrographs of Al-13Mg composite wires at different deformation true strains. The deformation processing resulted in a gradually finer microstructures of Al and Mg filaments. Many, but not all, of the Mg filaments displayed a convoluted ribbon shape at transverse section predicted by the plain strain mode [11]. These filaments inhibited the movement of dislocations, which is believed to be the reason for strengthening in the composites. In the longitudinal

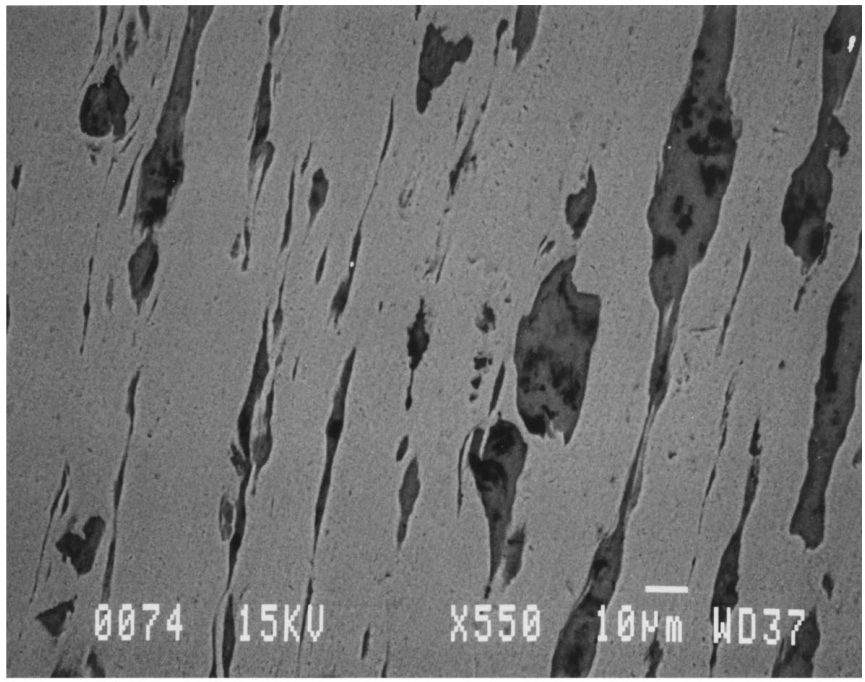

(a)

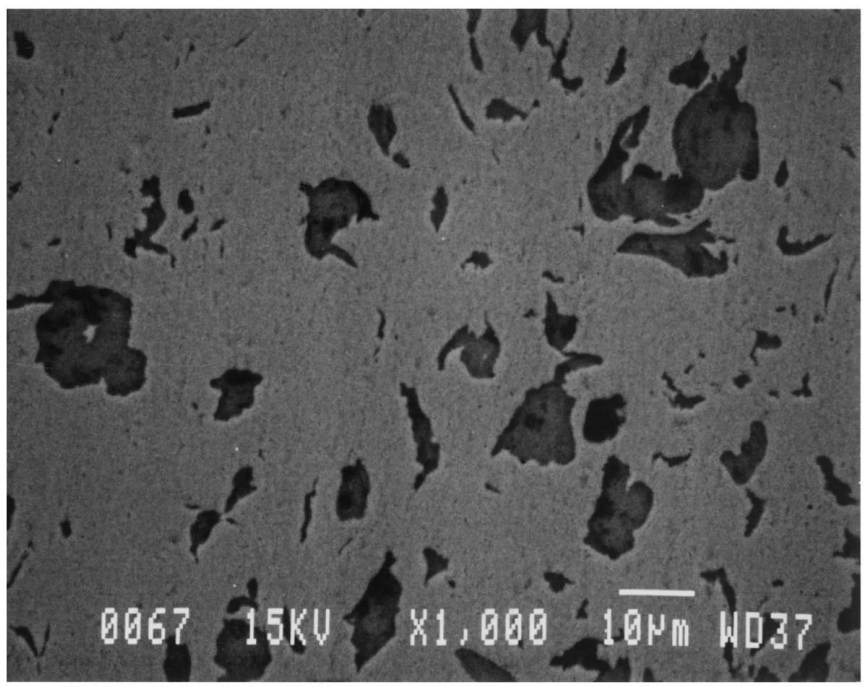

(b)

Figure 1 SEM micrographs of Al-13Mg deformation-processed to a true strain (η) of 2.77. (a) is longitudinal section; (b) is transverse section. The Al matrix is light gray, and the Mg is dark gray in these back-scattered electron images.

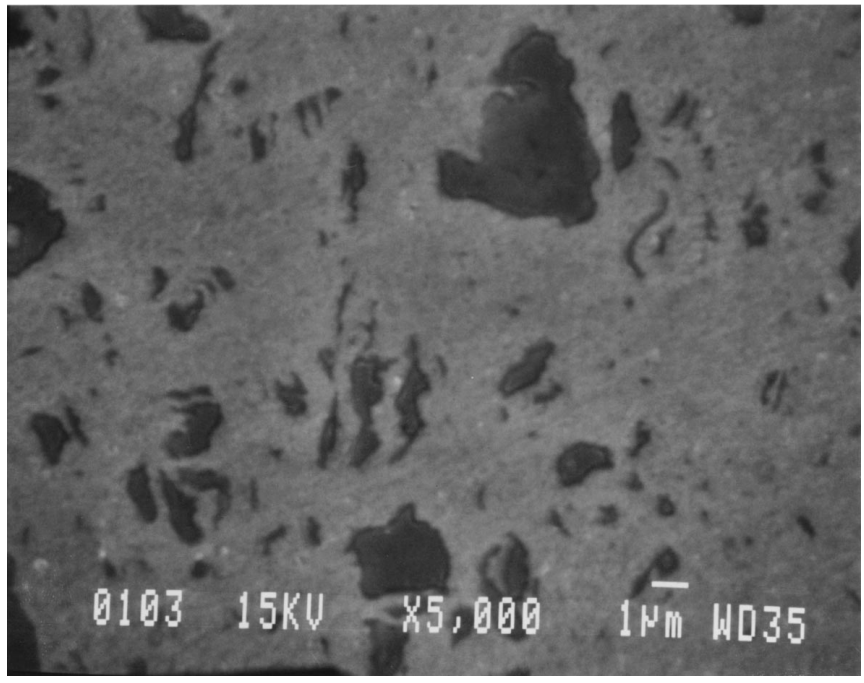

Figure 2 SEM micrograph of Al-13Mg deformation-processed to a true strain (η) of 10.10 and mounted in transverse section. The Al matrix is light gray, and the Mg filament is dark gray in the back-scattered electron image.

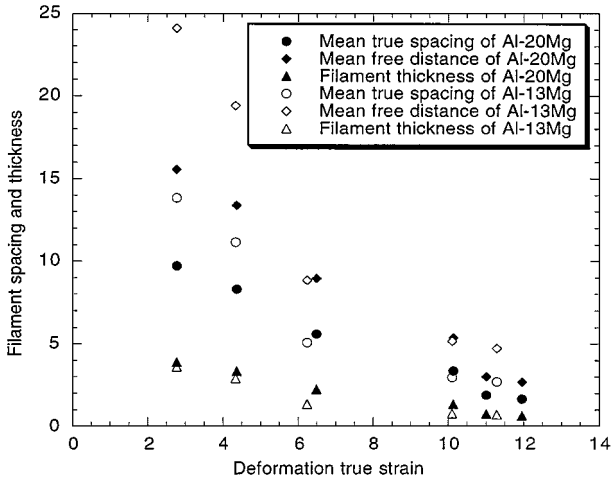

Figure 3 Mean true spacing, mean free distance and Mg filament thickness as a function of true strain for Al-20Mg and Al-13Mg.

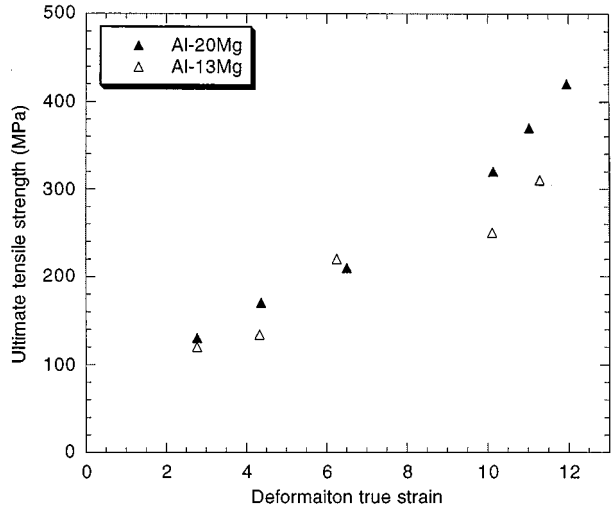

Figure 4 UTS as a function of deformation true strain for Al-20Mg and Al-13Mg.

section, the filamentary morphology and alignment of Mg with the wire axis is evident. Presumably, those Mg filaments that developed a convoluted ribbon shape did so because the HCP Mg developed a fiber texture during deformation processing which promotes plane strain. The microstructure of Al-20Mg is quite similar to that of Al-13Mg with some convoluted, ribbon shaped filaments.

The relationship between filament spacing and thickness and true strain is plotted in Fig. 3. The filament spacing and thickness decreases sharply with deformation processing. The difference between filament spacing and thickness also becomes smaller at higher deformation true strain. As observed previously [2], the filaments in the composites always decrease in thickness at a slower rate than the wire diameter. This means that the FCC matrix undergoes more deformation than BCC or HCP second phase filaments, which leads to the smaller difference between filament spacing and thickness at higher deformation true strain.

3.2. Strength of Al-Mg composite wires

Fig. 4 shows the relationship between ultimate tensile strength (UTS) and deformation true strain for Al-20Mg and Al-13Mg. The tensile strength of both Al-Mg composites increased as deformation processing proceeded. One significant feature of Fig. 4 was the relatively low increase in ultimate tensile strength when the specimen was deformed from $\eta = 6.24$ to $\eta = 10.10$ for Al-13Mg. When the Al-13Mg specimen was deformed, the rods were rebundled for a second extrusion as described in Section 2 to achieve a higher deformation value η. During the second extrusion of Al-13Mg, the separate rods did not initially bond well,

which lowers the strength of the composite. Not until the Al-13Mg exceeded $\eta = 10$ did the specimens appear to be a single monolithic wire.

Embury had modified the Hall-Petch model and indicated that there was an exponential relationship between strength and deformation true strain [12]:

$$\sigma = \sigma_0 + kd_0^{-1/2} \exp(\eta/4)$$

where σ is strength, σ_0 and k are constants, d_0 is the initial filament spacing, and η is deformation true strain. This assumption was confirmed by Russell [5] for deformation processed Ti-Y composite. Similarly, Sakai *et al.* [13] found that UTS $= 565 \exp(n\eta)$ for Cu-Ag composites where n is a factor that varies with Ag content. The exponential relationship between strength and deformation true strain can also be applied to the Al-Mg composites. It was found that:

$$\text{UTS} = 95.0 \exp(0.123\eta) \quad \text{for} \quad \text{Al-20Mg}$$
$$\text{UTS} = 92.4 \exp(0.107\eta) \quad \text{for} \quad \text{Al-13Mg.}$$

The fine filamentary microstructures were thought to impede the propagation of dislocations in both the matrix and the second phase, which leads to strengthening of the composites [14]. Previous studies on various DMMCs have quantified the relationship between filament spacing and ultimate tensile strength using a relation similar to the Hall-Petch type power function for yield strength. In Cu-20Nb axisymmetrically deformed DMMC's [15], UTS change was proportional to (Nb filament spacing)^x where x varied between -0.5 at low strains to -0.38 at high strains, while in axisymmetrically deformed Ti-20Y DMMC [5], UTS change was proportional to (Y filament spacing)$^{-0.37}$. In the Al-20Ti DMMC, UTS change was proportional to (Ti filament spacing)$^{-0.25}$ [8]. In the Al-Mg DMMCs of this study, the relationships between ultimate tensile strength and mean true spacing of Mg filaments are as follows (Fig. 5):

$$\text{UTS} = 585\sigma_t^{-0.61} \quad \text{for} \quad \text{Al-20Mg.}$$
$$\text{UTS} = 498\sigma_t^{-0.54} \quad \text{for} \quad \text{Al-13Mg}$$

where UTS = Ultimate tensile strength (MPa) and σ_t = mean true spacing of Mg filaments (μm).

The strengthening produced in these Al-Mg DMMC's may result from blockage of dislocation motion by the interfaces in the microstructure, i.e., the interface between Mg filaments and Al matrix. The large number of interfaces between Mg filaments and Al matrix inhibit the motion of dislocations, which gives rise to the strengthening of the deformation processed composites. The more the composites were deformed, the larger the total area of interfaces between the filaments and matrix and the smaller the filament spacing, leading to higher strength of the composites.

The results from Fig. 3 and Fig. 4 are replotted in Fig. 6 to show the dependence of the ultimate tensile strength of the Al-Mg composites on the mean free distance λ (or mean edge-to-edge spacing) and filament

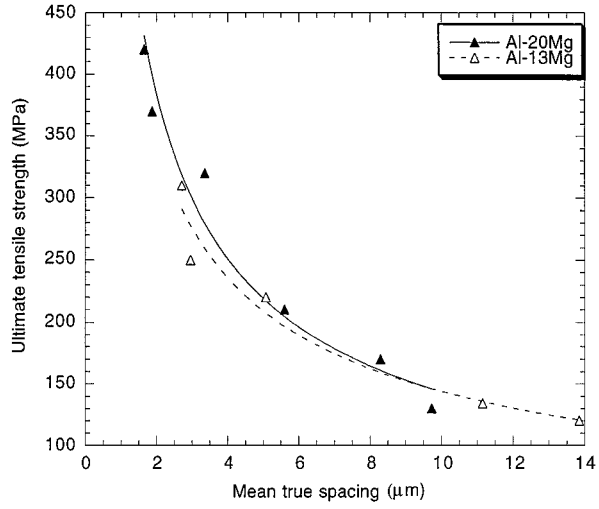

Figure 5 The dependence of ultimate tensile strength on mean true spacing for Al-20Mg and Al-13Mg.

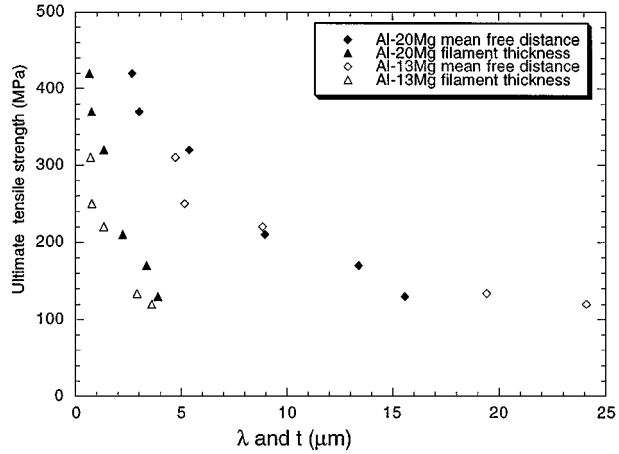

Figure 6 The dependence of ultimate tensile strength on the mean free distance λ and filament thickness t of Al-20Mg and Al-13Mg.

thickness t. The strength correlates with the filament thickness and mean free distance, with higher tensile strength at smaller mean free distance, and filament thickness.

The ultimate tensile strength are plotted against $\lambda^{-1/2}$ in Fig. 7 showing that while there is a good correlation with the Hall-Petch relationship, different curves are obtained for Al-20Mg and Al-13Mg as well as for the different compositions of each composite. The composite with higher Mg content (Al-20Mg) has the larger slope. This apparently occurs because the filament acts as a barrier to dislocation motion, and strength results from the blockage of dislocations. Al-20Mg has more Mg content than Al-13Mg, hence more filaments in unit transverse section area. This makes the motion of dislocations in Al-20Mg more difficult than Al-13Mg and results in the higher strength and larger slope for Al-20Mg.

3.3. Electrical resistivity of Al-Mg composites

The Al-13Mg composite ($\eta = 11.28$) was annealed at 538 K for 1 h in vacuum to form an Al-20Al_3Mg_2

TABLE I Electrical resistivity and ultimate tensile strength of Al-13Mg at $\eta = 11.28$ before and after annealing 1 h at 538 K and Al-20Mg

	Electrical resistivity (nΩ·m)	Ultimate tensile strength (MPa)	UTS : ρ ratio (nΩ·m : MPa)
Al-13Mg ($\eta = 11.28$) as-drawn (no annealing)	32.7	310	9.49
Al-13Mg ($\eta = 11.28$) after annealing	55.2	287	5.20
Al-20Mg ($\eta = 11.95$) as-drawn (no annealing)	35.8	420	11.73

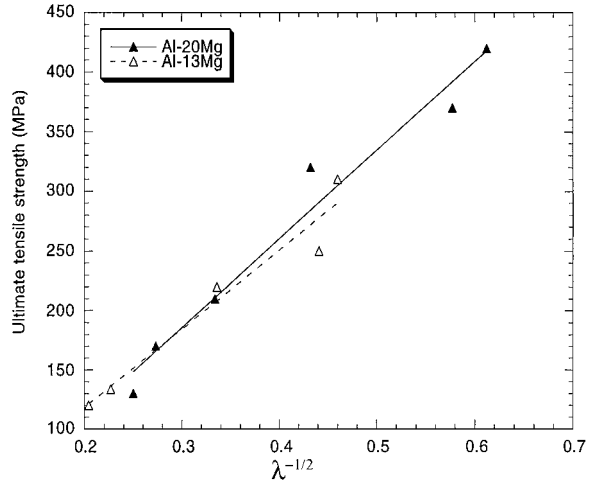

Figure 7 Hall-Petch relationship for Al-20Mg and Al-13Mg composites.

composite as confirmed by XRD. The electrical resistivity and ultimate tensile strength of Al-13Mg before and after annealing and Al-20Mg are tabulated in Table I.

The Al-13Mg and Al-20Mg have lower electrical resistivity compared with that of Al-20Ti (43 nΩ·m) [8]. It is not surprising that Al-13Mg composite has a low electrical resistivity. The matrix of the DMMC is 99.99% purity Al without solid solution atoms or GP zones. The electrical resistivity of pure Mg is 46 nΩ·m at 293 K, which is moderately higher than that of pure Al (28.2 nΩ·m at 293 K). Moreover, although the electrical resistivity of Mg is larger than that of Al, most of the cross sectional area of the DMMC is long strands of high purity Al, which allow the electrons to pass through with little scattering. The lower electrical resistivity makes the Al-Mg composites potential candidates for electrical applications. After heat treating, some Mg diffused into the Al matrix and formed a solid solution. Other Mg reacted with Al and formed the intermetallic compound. Both phenomena contribute to the increase of electrical resistivity. It remains for future study to deform the composites to higher deformation true strain and to achieve higher UTS : ρ ratio.

4. Conclusions

1. Deformation processing can produce Al-20Mg and Al-13Mg composites with a maximum deformation true strain of 11.95 and 11.28 respectively.

2. Most of the Mg second phase adopts a convoluted, ribbon shape filamentary morphology after deformation. Both the size and spacing of these filaments decrease as deformation progresses.

3. With increasing deformation, the strength of Al-Mg composites increases exponentially with true strain.

4. Strengthening in Al-Mg composites arises from the Mg filaments acting as barriers to dislocation movement. The heavy deformation results in a reduction in Mg filament spacing (σ_t) and the dependence of strength (MPa) on this spacing is:

$$\text{UTS} = 585\sigma_t^{-0.61} \quad \text{for} \quad \text{Al-20Mg}$$
$$\text{UTS} = 498\sigma_t^{-0.54} \quad \text{for} \quad \text{Al-13Mg}.$$

Acknowledgements

This work was performed at Ames Laboratory, operated for the US Department of Energy by Iowa State University under contract no. W-7405-Eng-82. The authors would like to thank the Ames Laboratory for technical support and academic discussions. Special thanks is given to I. Anderson for providing the GARS Al powder used in this study and to L. Lincoln, L. Jones, P. Wheelock of the Ames Laboratory Materials Preparation Center for preparing the materials used in this study. Thanks also goes to Joel Harringa for his assistance in electrical resistivity measurement.

References

1. J. BEVK, J. P. HARBISON and J. L. BELL, *J. Appl. Physics* **49**(12) (1978) 6031–6038.
2. W. A. SPITZIG, A. R. PELTON and F. C. LAABS, *Acta Metall.* **35**(10) (1987) 2427–2442.
3. J. D. VERHOEVEN, F. A. SCHMIDT, E. D. GIBSON and W. A. SPITZIG, *Journal of Metals* **38**(9) (1986) 20–24.
4. C. L. H. THIEME, S. POURRAHIMI and S. FONER, *Scripta Met & Mat* **28** (1993) 913–918.
5. A. M. RUSSELL, L. S. CHUMBLEY, T. W. ELLIS, F. C. LABBS, B. NORRIS and G. E. DONIZETTI, *J. Mater. Sci.* **30** (1995) 4249–4262.
6. A. M. RUSSELL, T. W. ELLIS and L. S. CHUMBLEY, *ibid.* **30** (1995) 2070–2076.
7. J. A. JENSEN, A. M. RUSSELL, T. W. ELLIS and L. S. Chumbley, "Light Metals 1995," edited by J. Evans (TMS, Warrendale, PA, 1995) pp. 1367–1374.
8. A. M. RUSSELL, T. LUND, L. S. CHUMBLEY, F. C. LABBS, L. L. KEEHNER and J. L. HARRINGA, *Composites: Part A*, accepted June, 1998, in press.
9. B. W. CHRIST, *ASM Metals Handbook*, **8** (1985) 28–32.
10. E. E UNDERWOOD, "Quantitative Stereology" (Addison-Wesley, Reading, MA, 1970) pp. 80–93.
11. W. F. HOSFORD JR., *Trans. Met. Soc.* AIME, **230** (1964) 12–15.
12. J. D. EMBURY, *Scripta Metall.* **27** (1992) 981–986.
13. Y. SAKAI and H. J. SCHNEIDER-MUNTAU, *Acta Mater.* **45**(3) (1997) 1017–1023.
14. W. A. SPITZIG, J. D. VERHOEVEN, C. L. TRYBUS and L. S. CHUMBLEY, *Scripta metall.* **24** (1990) 1171–1174.
15. J. D. VERHOEVEN, L. S. CHUMBLEY, F. C. LAABS and W. A. SPITZIG, *Acta Metall.* **39**(11) (1991) 2825–2834.

Received 2 March
and accepted 5 May 1999